



Supplementary Materials for

Hypoxia Triggers Meiotic Fate Acquisition in Maize

Timothy Kelliher* and Virginia Walbot*

*E-mail: tkellih1@stanford.edu (T.K.); walbot@stanford.edu (V.W.)

Published 20 July 2012, *Science* **337**, 345 (2012)

DOI: 10.1126/science.1220080

This PDF file includes:

Materials and Methods

Figs. S1 to S14

Tables S1 to S4

References (28–33)

Materials and Methods

qRT-PCR

mac1 was cloned and the gene encodes the closest maize homolog to TPD1, a putative secreted ligand (7). qRT-PCR was used to quantify the expression of *Mac1*. Samples included 1 mm tassel (containing spikelet pair meristems), 5 mm tassel (containing spikelet meristems), and 10 mm tassel (containing stamen primordia), and 50, 150, 250, 400, and 700 μm fertile anthers (primordia, archesporial (AR) cell specification, secondary parietal layer and endothecium specification, mitotic proliferation, middle layer and tapetum formation). Stages are described in figure S1E. Samples of 200 μm *mac1* (excess AR) and *msca1* (zero AR) mutant anthers were also tested. RNA was extracted with TRIzol reagent (Ambion, Austin, Texas) from anthers snap frozen in liquid nitrogen within 20 min of dissection, except in the case of laser microdissected cell types (described below). Extraction was followed by chloroform/isopropanol precipitation and resuspension in RNase-free H_2O . All RNA samples were DNase treated with RNase-free DNase (Qiagen, Venlo, The Netherlands), purified on an RNeasy mini spin column (Qiagen), and quantified on a Nanodrop 1000 spectrophotometer (Thermo Scientific, Waltham, MA).

In addition, we tested *Mac1* expression in a cell-type specific manner by performing qRT-PCR on laser-microdissected AR and somatic (SPL + endothecium) samples isolated from 300 and 700 μm fertile anthers. Anthers were fixed in 3:1 ethanol: acetic acid solution, then cryoprotected in 15% sucrose/PBS and embedded in optimal cutting temperature compound (Ted Pella Inc., Redding, CA). They were then frozen, cryo-sectioned and attached to slides with a Cryojane (Electron Microscopy Sciences, Hatfield, PA). After an ethanol to xylenes dehydration series, 10-12 μm sections were microdissected using the Zeiss P.A.L.M. Laser Microbeam (<http://www.palm-microlaser.com>) for recovery of cell types. RNA was isolated using the PicoPure RNA extraction kit (Arcturus Molecular Devices, Mountain View, CA), with on-column DNase treatment and resuspension in RNase-free dH_2O as described above for whole anther RNA.

After quantification, whole anther and microdissected RNA biological replicates were used for cDNA synthesis using the SuperScript III First-Strand Synthesis System for RT-PCR (Invitrogen, Carlsbad, CA) using oligo (dT)₂₀. Each qRT-PCR reaction was performed in technical triplicate on cDNA derived from 8-10 ng starting mRNA with SYBRGreenER qPCR SuperMix (Invitrogen) on an Opticon 2 thermocycler (Bio-Rad, Richmond, CA) and fluorescence values were analyzed using PCR miner (<http://www.ewindup.info/miner/version2/>) to account for primer efficiencies. *Mac1* transcript was detected using a forward primer in exon 1 (5'-AACCCTACTGCGAAACAAC-3'), and a reverse primer that spans exons 2 and 3 (5'-CGAGAATCCTGCGTCCTGAT-3') so as to avoid amplifying contaminating genomic DNA. *Cyanase* was used as a control gene (Forward: 5'-GGTGGTCACATTTGATGGG-3'; Reverse: 5'-CTGAGCCCGATACCAACC-3'). The

ratio of *Mac1* to *Cyanase* was used to normalize expression among biological samples. Each sample type was tested in biological triplicate.

Microarray analysis

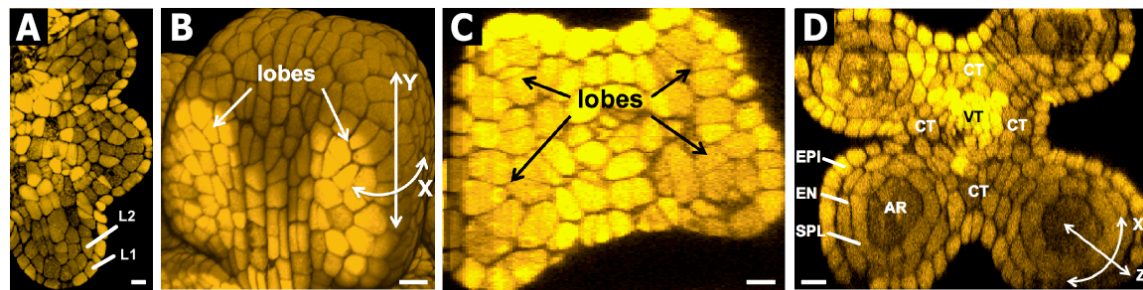
Two microarray experiments were performed. The goal of the first experiment was to test the expression profiles of *mac1* AR cells with respect to a set of 297 meiosis-associated genes (12). AR cells microdissected from *mac1* anthers were compared to laser microdissected AR from fertile (*mac1* heterozygous) sibling anthers. Anthers were at the 5-cell layer stage (1.0 mm anther length), after all AR mitoses are completed during a period of AR expansion. In a separate experiment designed to profile the early archesporial cell transcriptome, 600-700 μm fertile whole anthers were compared to laser microdissected AR cells from the same stage. To control for growth condition differences between plants, whole anthers and microdissected anthers were collected from the same individual plants to permit a direct comparison between anthers of the same tassel.

Both experiments were done in biological duplicate, each with two technical replicates (dye swap); 50 ng total RNA was used for amplification according to the Agilent Two-Color Microarray-Based Gene Expression Analysis Low Input Quick Amp Labeling Protocol (version 6.5, May 2010) (Santa Clara, CA) and hybridized in 4x44K format (Part number: G2519F; Design ID: 016047). Background fluorescence cut off was set and data were normalized as described (28). Genes were identified as being above background based on expression at least 3 standard deviations above the mean intensity of negative control probes (false discovery rate $p < 0.001$).

Tassel manipulations

The oxygen probe was an Oxygraph Tx3 (NTH-Pst1-L5-NS40-0.8-YOP) obtained from Presens (Regensburg, Germany, <http://www.presens.de>). All chemicals were obtained from Sigma Chemical Co. (St. Louis, MO) and dissolved in water at the indicated molarities and injected using a 26 gauge needle into the airspace surrounding the immature tassel. Cellular redox was perturbed chemically by injecting 1 mL of 1 mM H_2O_2 or 10 mM KI (a peroxide scavenger). Two promoters of ROS were tried: 200 μM PTIO and 100 μM L-NNA. 20 μM SNP, a ROS inhibitor, was also employed. A water injection showed no difference from needle puncture alone, so the latter was used as control for injections.

Confocal imaging, and EdU and PI staining were performed as described previously (13). Measurements were made with the length tool in the Volocity software package (Perkin Elmer, version 5.1.1, Waltham, MA).



E	stage or process	anther length (µm) (initial / completed)	hours after stamen initiation (initial / completed)	internal lobe cell types present during stage range
	Stamen initial	0 / 70	0 / 48	L2
	Anther lobing	70 / 120	48 / 96	L2-d
	L2-d central cells	120 / 160	96 / 108	L2-d, presumptive AR (central L2-d)
	AR specification	120 / 200	96 / 122	L2-d, presumptive AR, first differentiated AR (central, present in larger sizes only)
	AR differentiation	160 / 220	108 / 126	presumptive AR (tip & base), differentiated AR, L2-d, SPL & EN initials (central, present in larger sizes only)
	L2-d periclinal divisions	180 / 280	114 / 138	presumptive AR (tip & base), differentiated AR, L2-d, SPL & EN
	Four mitotic cell layers	280 / 550	138 / 174	AR, SPL & EN
	SPL periclinal divisions	550 / 700	174 / 198	AR, EN, ML, TA
	Prophase I of meiosis	1500 / 2000	240 / 268	meiocytes, EN, ML, TA

Fig. S1

Introduction to early anther development and timeline of events. Anther development begins with three stamen primordia initiating from a floret meristem (A). Three 55-µm dome-like stamen primordia are visible in this longitudinal optical section of a maize tassel floret. The L1 layer gives rise exclusively to the epidermis, while the L2 subepidermal layer generates the internal lobe tissues, including both somatic and germinal cell types. This dome shape gradually converts to the butterfly shape with lobe protrusion (B). In this 3D composite of a 100-µm anther, two adaxial lobes are visible along with the filament at the bottom of the image. Axes are as follows: Y, longitudinal; X, circumferential; and Z, radial. (C) Transverse reconstruction of a 110-µm anther showing budding lobes and central vasculature. All lobes have L2-d cells and no central (presumptive archesporial [AR]) cells are seen. (D) After two days and a 3X increase in anther length and girth accomplished by cell division with a constant average cell size, AR cells are located in the middle of lobes, surrounded by two concentric rings of

somatic cells, the secondary parietal layer (SPL) and endothecium (EN), enclosed by the epidermis (EPI) and connective tissue (CT). All of these cell types are visible in this transverse reconstruction of a 300 μm anther. Over the next seven days AR cells proliferate, differentiate as pollen mother cells, and initiate meiosis. Meanwhile each somatic cell type exhibits a distinctive pattern of proliferation and expansion (13). Multipotent SPL cells divide periclinally once and daughter cells terminally differentiate into middle layer and tapetum. The latter surrounds the meiocytes (29) and supports later pollen maturation. The defining characteristics of AR cells with our stain under confocal microscopy are enlargement, amorphous shape, a small gap between cells, and a dark, diffuse cytoplasmic stain. In transverse sections for light microscopy, there is no gap: AR cells have thin adjoining walls. The difference between the two types of microscopic observation probably results from the fixative used (ethanol in the propidium iodide / confocal protocol; formaldehyde for light microscopy). Scale bar = 15 μm . (E) Key developmental events of wild type W23 inbred anther development spanning stamen initiation through meiosis. Each developmental stage or process is assigned a range of anther lengths in micrometers and time after stamen initiation in hours. Also listed on the right are the different internal lobe cell types present during each range. Many of the stages overlap because when the anther is viewed longitudinally, the center is more advanced than the base and tip. ML, middle layer; TA, tapetum.

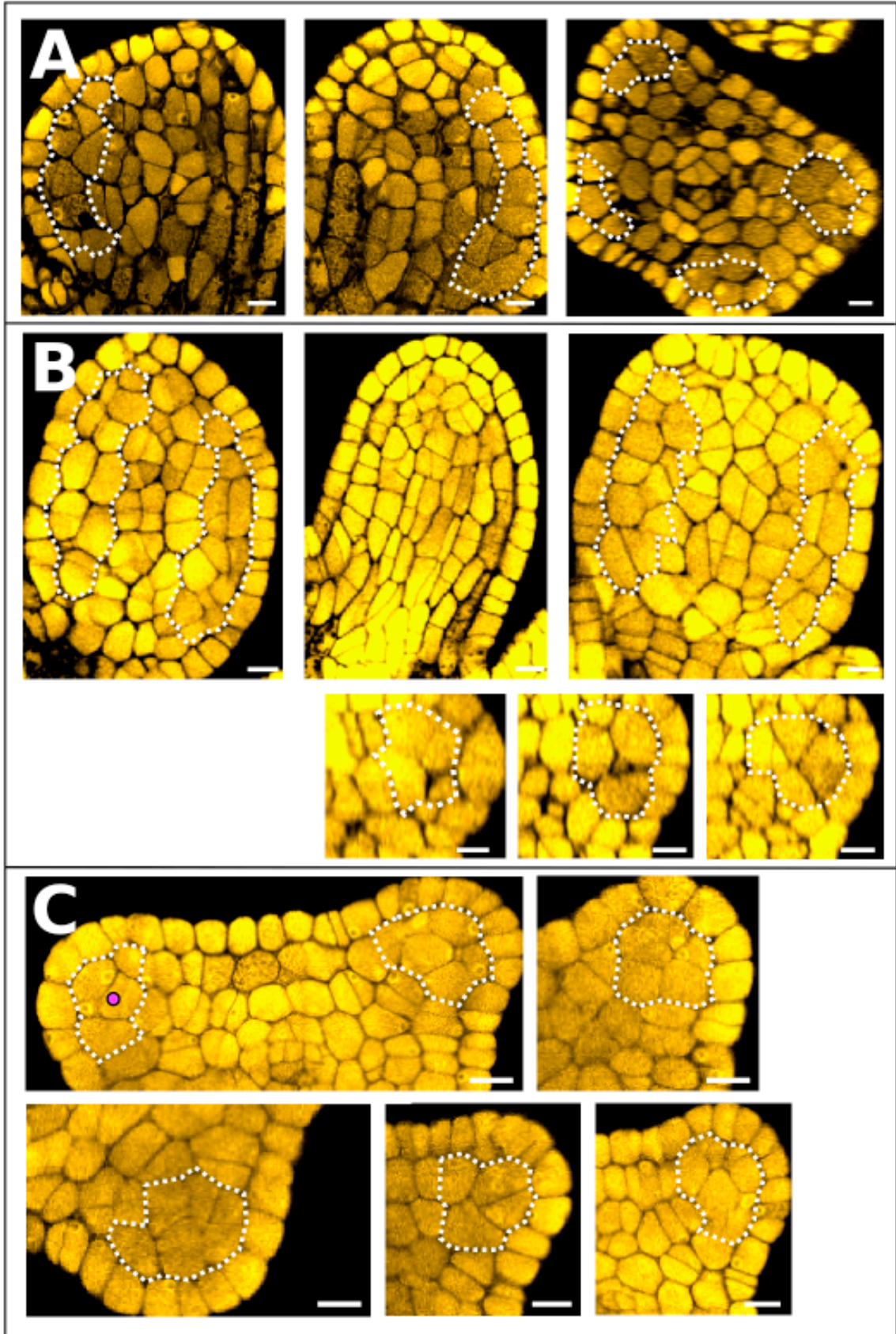


Fig. S2

Early anther lobes are multicellular and there is no evidence for an enlarged hypodermal cell as described in the lineage model of germinal cell fate specification (see below). L2-d progenitor cells (white outline) will give rise to either somatic or germinal cell types or both. (A) 90- μm anther: longitudinal images (*left, center*) and transverse reconstruction (*right*). The only cells outlined were within the lobe bulge in all views. (B) 105- μm anther showing longitudinal images of adaxial lobes (*left*), central vasculature composed of organized cell columns (*center*), and abaxial lobes (*right*). *Below*, three transverse reconstructions of the same anther showing single lobes. (C) 118- μm anther, transverse images of different parts of the four lobes. One of the lobes (*top left*) contains a single presumptive archesporial (AR) cell (pink dot) derived from division of an internal L2-d progenitor. We designate this an AR cell because of its position surrounded completely by other L2-d lobe cells in the complete series of confocal images. Scale bar = 15 μm .

Several conventions have arisen to name the cells in immature anthers, based on different assumptions about their roles in anther ontogeny. The textbook view is that lineage defines cell fate and that there exists an enlarged hypodermal cell in the four corners of anther primordia that divides asymmetrically to establish the somatic and germinal lineages and fates in a single division. The classical nomenclature of “hypodermal cell”, “primary parietal cell”, and “primary sporogeneous cell” assumes this lineage model of anther cell type specification. As this report presents the first three-dimensional reconstruction of anther development during the period of reproductive fate specification and our results contradict the classical lineage view, we propose new vocabulary to reflect the developmental patterns observed. We prefer L2-d to describe the multipotent cells which can give rise to any of the internal lobe cell types, and presumptive archesporial cells to describe cells that end up in the center of the lobe in early anthers (all of which are central L2-d cells that acquire an archesporial cell fate). The archesporial cells are instructive in directing neighboring cells to restrict from pluripotent L2-d to two cell types (endothecium and secondary parietal layer) as a result of periclinal division. Our results indicate a sequential specification: initially all L2-d, then archesporial and L2-d, and then archesporial, endothecium and secondary parietal layer.

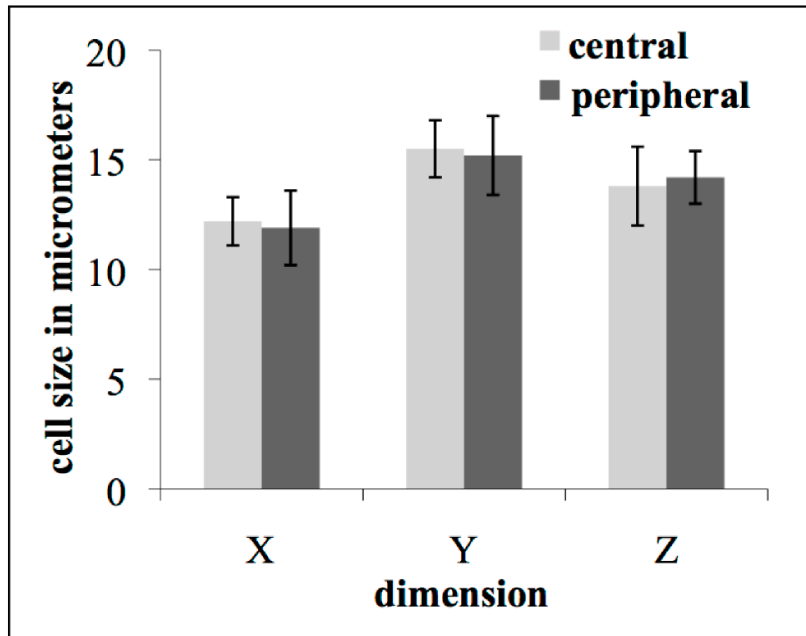


Fig. S3

Archesporial-generative divisions are symmetric. The dimensions of presumptive archesporial cells and somatic sisters were equal in W23. Measurements were made with the length tool in Volocity in the circumferential (X), longitudinal (Y), and radial (Z) dimensions (N = 48). Values are averages +/- s.d. indicated by the error bars. There was no significant difference in any dimension.

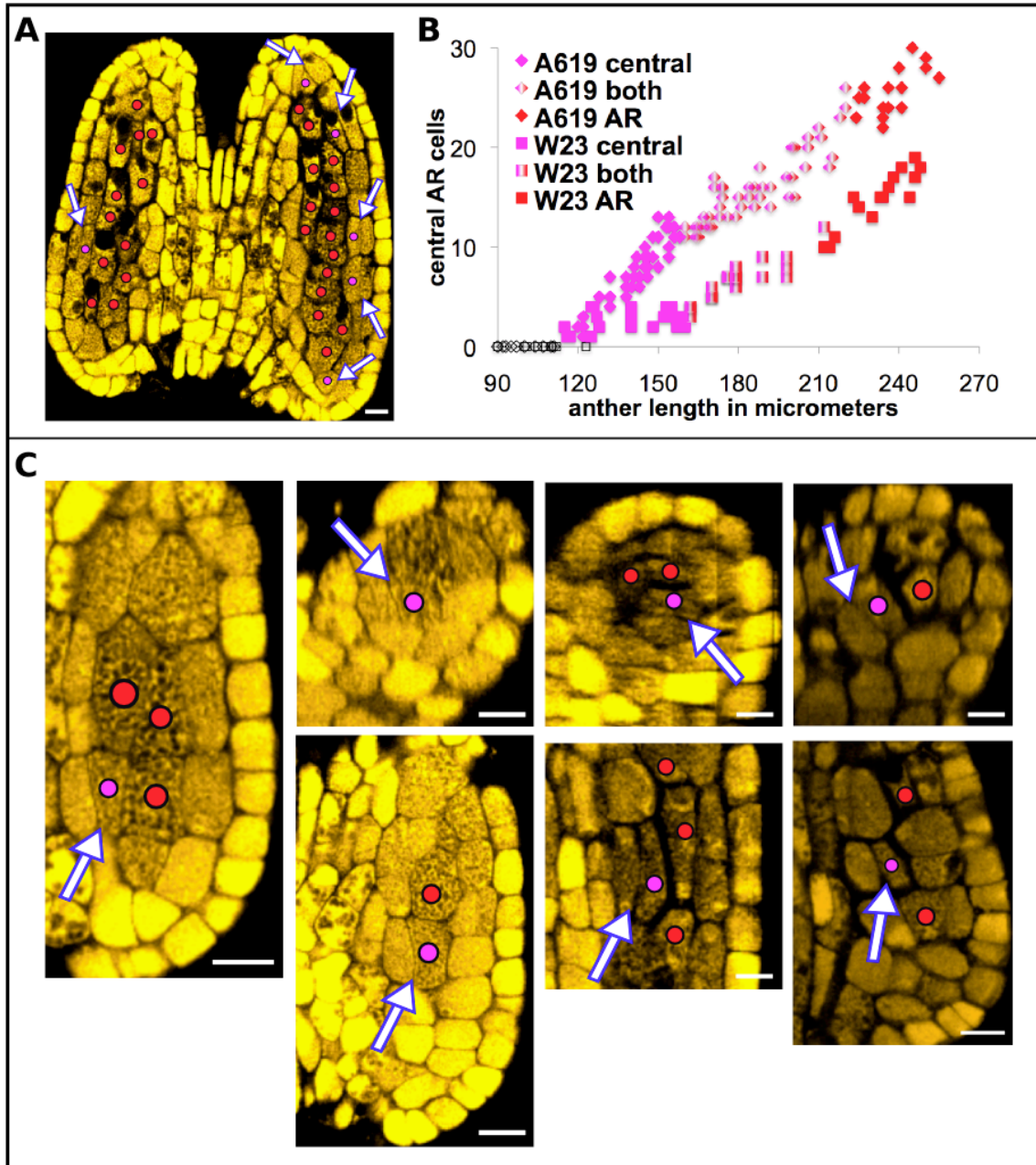


Fig. S4

After morphometric analysis, inbred A619 had identical developmental progression but extra archesporial cells compared to inbred W23. A619 was chosen for comparison with W23 because it has a slower flowering progression and fewer flowers per tassel than W23. The general developmental patterns observed were identical between the two inbreds: multiple L2-d progenitors occupied early lobes, there was no evidence for a hypodermal cell, and presumptive archesporial cells derived from apical, lateral, and basal positions in the lobe. **(A)** 170- μ m anther from A619. In A619 there are ultimately two archesporial cell columns produced during the specification period, compared to just one in W23. **(B)** Quantification of archesporial cells over the period of germinal cell

specification in both A619 and W23. There were 2X more archesporial (AR) cells in A619 than W23 at each stage. In both inbreds, the first presumptive archesporial cells born are surrounded by L2-d with additional presumptive archesporial cells being specified from successive divisions in different progenitors in the center, base and tip. These observations confirm the multiclonal origin of germinal cells in each lobe. As in W23, archesporial cell specification lasted from 120 to 220 μm with morphological differentiation apparent at 160 μm in the central most archesporial cells of the column. In particular, the range from 160-220 μm is complex because at the same time that archesporial (AR) cells are enlarging centrally and periclinal divisions are occurring in the encircling L2-d ring to give rise to secondary parietal layer (SPL) and endothecium (EN) initials, there are new presumptive AR being born from L2-d progenitors at the tapered tip and base of the anther. Somatic differentiation initiated and completed at the same stages as W23. (C) The inner column of AR in A619 primarily derives from divisions in lateral or basal positions. These divisions simultaneously give rise to central presumptive AR and subtending somatic daughter cells adjacent to the connective tissue. *Left*, longitudinal section with presumptive AR born from an internal progenitor. Differentiated archesporial cells are visible above and to the right of the presumptive archesporial cell. *Top right*, three transverse reconstructions with internal archesporial births into the central column where archesporial cells are found slightly later. *Bottom*, three longitudinal images with internal archesporial births into central columns already containing archesporial cells. Pink dots, presumptive archesporial cells; red dots, differentiating archesporial cells; white arrows, cell walls separating presumptive archesporial and somatic sister cells. Scale bar = 15 μm .

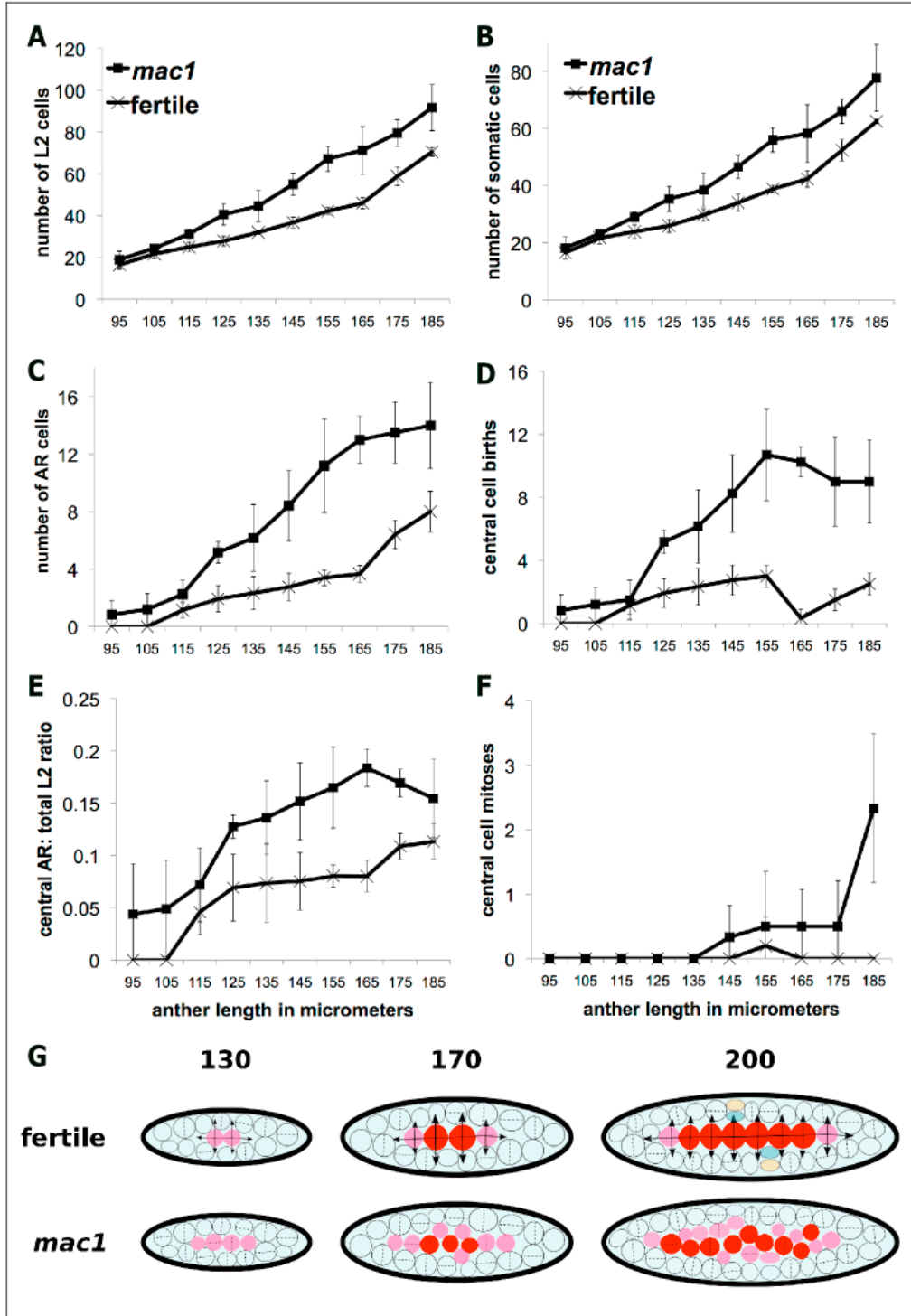


Fig. S5

Male sterile *mac1* and fertile sibling cell counts detail the excess L2-d and archesporial (AR) cells characteristic of the *mac1* phenotype. Each point represents the average count of at least 16 lobes +/- s.d. (A) *mac1* had supernumerary L2-d cells in the smallest anthers imaged, and the gap between sterile and fertile widened until 165 μm, when it

began to close. Excess cells in *mac1* were located in the somatic ring **(B)** as well as the central presumptive archesporial cell column **(C)**. **(B)** As the somatic bilayer formed in fertile anthers (>180 μm anther length) the difference in somatic cell number decreased, and by 230 μm (not shown) fertile overtook *mac1* because *mac1* lobes continued to contain only a single L2-d layer. **(C)** Central presumptive archesporial cells were found in smaller anthers in *mac1* than in fertile (including in some 95 μm long anthers). This is a consequence of excess L2 progenitor proliferation (these cells were also smaller than in fertile (data not shown)), resulting in more cells positioned internally surrounded completely by L2-d neighbors. **(D)** Furthermore, more additional archesporial cell births occurred in *mac1* than in equivalently sized fertile anthers in 125-185 μm lobes. Many of the extra archesporial-generative divisions were periclinal divisions in the ring surrounding differentiated archesporial cells, a case rarely found in fertile anthers. **(E)** The ratio of archesporial cells to total L2 is indicative of excessive proliferation (given the circular architecture of the tissue in cross-section, additional cells must be located in the middle, becoming a higher fraction of the total cells in *mac1* than in fertile). **(F)** *mac1* archesporial cells are mitotic at early stages, a trait observed only rarely in fertile lobes. **(G)** Longitudinal diagrams of early fertile and *mac1* lobe development (numbers indicate anther length in micrometers). Pink cells are just specified AR and red cells are differentiated AR. Arrows indicate the proposed direction of MAC1 protein secretion from archesporial cells to neighboring L2-d tissues.

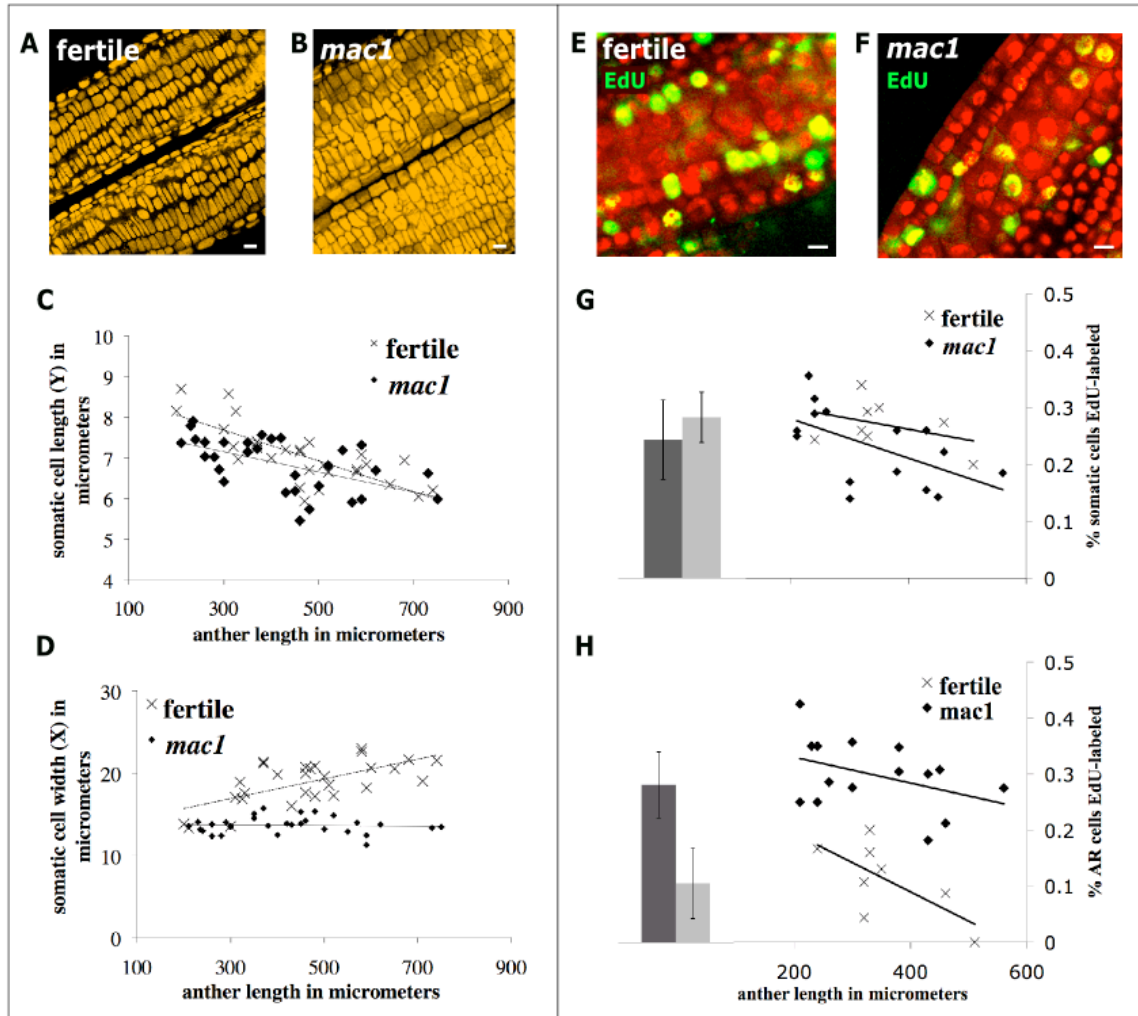


Fig. S6

MAC1 does not influence somatic proliferation rate as a whole, but rather directs the singular periclinal division of L2-d neighbors. Two *Arabidopsis* mutants are similar to *mac1*: the LRR receptor kinase EXS/EMS1 and its putative secreted ligand TPD1, a homolog of rice OsTDL1A (7, 30-33). These molecules are proposed to define a signaling module responsible for tapetal fate specification and/or proliferation (9). Unlike *mac1*, *tpd1* and *ems1* mutants typically form endothecium and secondary parietal layer but middle layer and tapetum specification is faulty (4, 11). In maize, does MAC1 promote differentiation and anticlinal proliferation of presumptive secondary parietal cells, as proposed for the role of TPD1 in tapetal development (9), or more specifically control the critical periclinal division?

Cell counts and measurements indicated that anticlinal proliferation of the faulty somatic layer is excessive in *mac1* compared to either the fertile endothecium or SPL, because the single layer *mac1* soma had a cell census similar to the sum of endothecium and secondary parietal layer in fertile. (A-B) Fertile endothecium illustrated normal cell numbers (A) and *mac1* subepidermal layers contained excessive cells (B). The

endothelial layer in fertile had ~12-14 very wide cells around the lobe at reproductive maturity (13). In *mac1* ~ 20 - 25 somatic cells occupied this circumference. (C, D) In addition, *mac1* somatic cells were smaller than either secondary parietal layer or endothecium reflecting increased anticlinal division to sustain anther growth. (C) Endothecium / subepidermal cell length (distance along longitudinal (Y) axis) was equivalent. (D) Somatic cell width (circumferential (X) axis) was smaller in *mac1*, as a result of excessive anticlinal divisions. Each point represents the average of least 50 cells in a single lobe. Eventually, a partial second layer formed in *mac1* around 700 μm , five days late, but appeared dissimilar to the secondary parietal layer, middle layer, and tapetum. This is similar to aspects of TPD1 / EMS1 phenotypes in *Arabidopsis*, but in those mutants a full secondary parietal layer is present initially, while in *mac1* no secondary parietal layer was ever formed. Interestingly, the *exs* mutant in the C24 background has only a single somatic layer as is found in *mac1* (30).

Does mitotic rate of the somatic and germinal cells change in the *mac1* mutant? (E-F) 10 μM EdU was injected into tassels during the phenocritical period, and 6 hours later 200-600 μm anthers were stained (13). The EdU stain showed excessive staining in *mac1* archesporial cells, indicative of a faster mitotic rate. Red, propidium iodide; green, EdU. (G-H) Quantification of EdU staining in fertile and *mac1* somatic layer(s). Each dot represents a single lobe, from which all the cells were counted. EdU staining was even and distributed equivalently along the length of the lobe, because anthers lack an intercalary meristem. The bars represent averages of the lobes examined \pm s.d. (G) Combining the cell counts for the EN and SPL layers together for fertile, the percentage of somatic cells that were EdU positive is slightly greater than in *mac1* but the difference is not significant. (H) The percentage of EdU+ archesporial cells was significantly greater in *mac1* than in fertile (Student's T-test, $p < 0.01$). Scale bar = 15 μm .

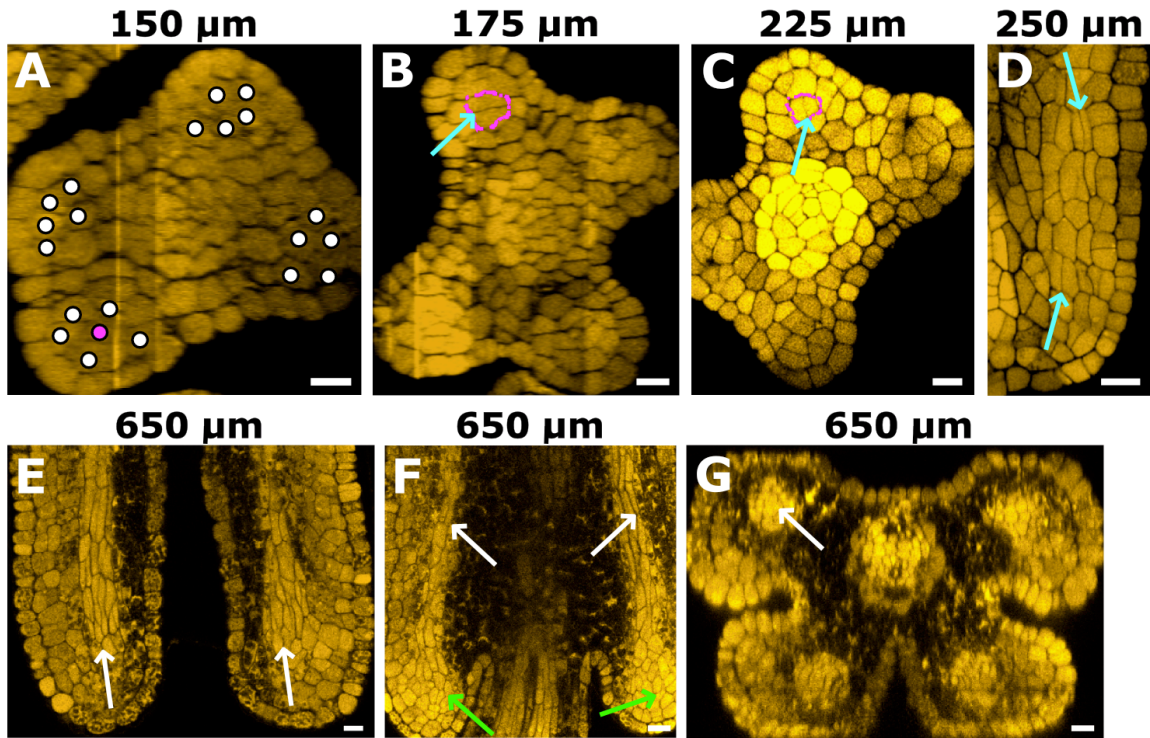


Fig. S7

Sterile *msca1* anthers failed to differentiate archesporial cells correctly and had none of the normal lobe cell types. Initially, anthers appeared normal (A), with white dots marking L2-d cells. At the same stage that archesporial cells enlarge in fertile, the *msca1* central presumptive archesporial cells (pink dot) failed to enlarge. (B-D) They instead continued to proliferate (blue arrows) making longitudinal divisions to create long, columnar cells that differentiated as vascular bundles. (D-G). These bundles (white arrows) did not connect with the central vasculature of the stamen, but instead terminated at the tips and base into a mass of parenchyma-like cells (green arrows) (F). Scale bar = 15 μm.

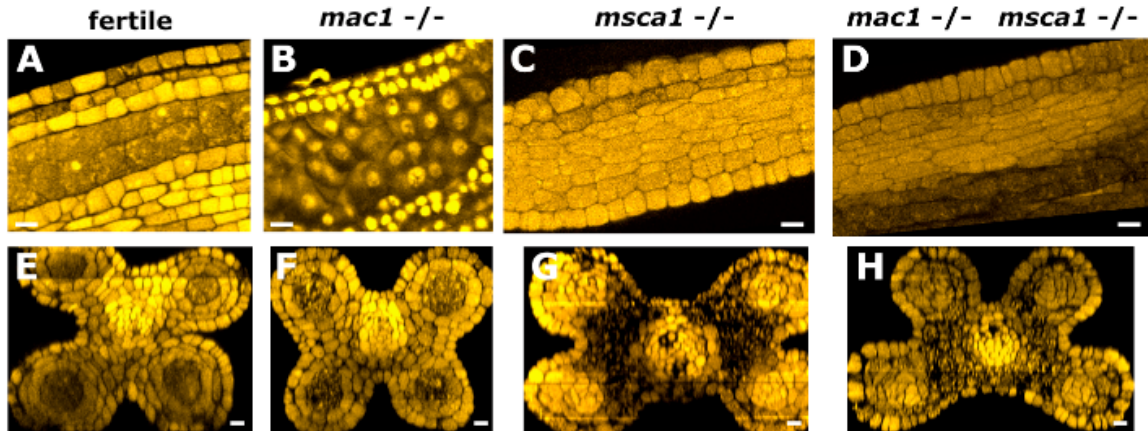


Fig. S8

msca1 is epistatic to *mac1*. (A-D) Longitudinal images of single lobes. (E-H) Transverse Z-stack reconstructions showing the butterfly cross-section. (A,E) Fertile anther at 300 μm . The lobe cell layers from the outside in are epidermis, endothecium, secondary parietal layer, and archesporial. (B,F) *mac1* anther with EPI, a faulty somatic layer with occasional periclinal division resulting in a one cell wide bilayer, and excess archesporial cells. The longitudinal image (B) is from a 600- μm anther while the transverse reconstruction (F) is from a 280 μm anther. (C,G) *msca1* anthers lack all normal internal cell types and instead lobes contain vascular bundles and parenchyma-like cells. (D,H) The double mutant looked just like *msca1*. Scale bar = 15 μm .



Fig. S9

To determine oxygen concentration, we inserted a needle-borne probe at several developmental stages. After measuring percent O₂, plants were opened to confirm needle position in the airspace and measure anther size. Measurements were ~1.4% at the 2 cm tassel stage at the stage when archesporial specification occurs, and at 12 cm increments above the tassel they were 4%, 8%, 16% and finally 20% O₂ near the top. Thus, there is an oxygen gradient in the whorl, with a hypoxic atmosphere surrounding the tassel. (A) Oxygen probe set up with needle inserted through the leaf whorl at the level of the tassel and positioned within the internal airspace. (B) Hose threaded down into leaf whorl for gas delivery avoiding the wounding response. (C, D) Gas delivery through a 26-gauge needle positioned directly into the airspace.

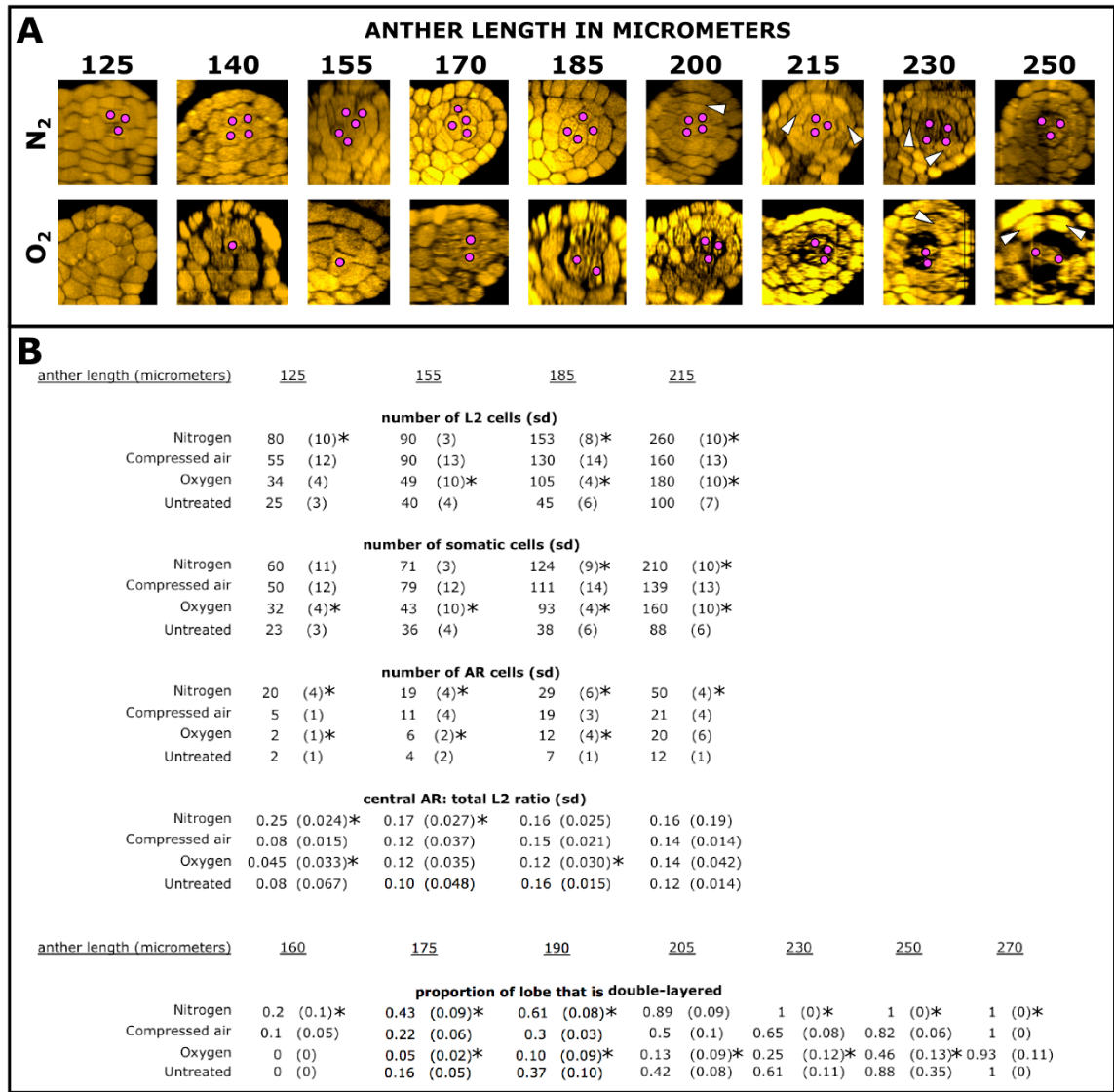


Fig. S10

Gas delivery via needle positioned directly into the airspace confirmed the phenotypes observed in the hose application. Compressed air (20% O₂) application, a mild oxygenation treatment, controlled for wounding and/or desiccation effects. (A) Transverse reconstructions demonstrate precocious and excessive archesporial (AR) cell specification (pink dots) and early somatic bilayer formation (white arrows). Scale bar = 15 μm. (B) (top) Compared to compressed air, N₂ promoted L2-d and somatic cell proliferation at three out of four size classes while O₂ decreased counts early. Excess presumptive archesporial (AR) cells are present in N₂-treated lobes at all stages while O₂ had significantly fewer compared to compressed air at all but the largest size class. AR: total L2-d ratio was dramatically higher in N₂ and slightly lower in O₂ than compressed air at early size classes. (bottom) Quantification of the secondary parietal layer / endothecium formation confirms findings from the hose delivery protocol. Stars represent significance compared to control by Student's T-test (p < 0.01).

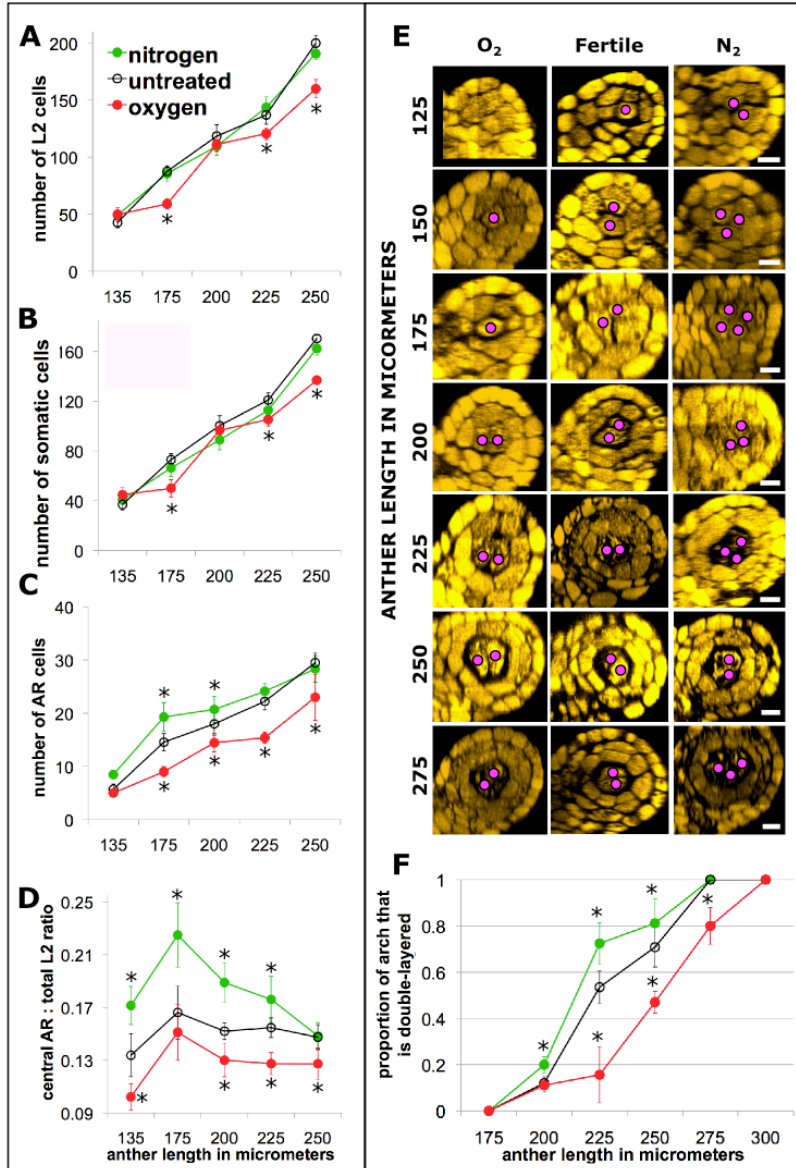


Fig. S11

24 hour hose application on A619 inbred recapitulated results, but with milder effects on cell proliferation. To confirm results from W23, these treatments were performed on the A619 inbred, which has double the archesporial (AR) cell count. Total L2 cell counts (**A**) and somatic cells (**B**) were significantly lower in O₂ treatment at three of the five size classes compared to both untreated fertile and N₂ treatment. (**C**) The total number of presumptive and differentiated AR cells was significantly elevated in two N₂ size classes, while O₂ treatment resulted in fewer AR in almost all size classes. (**D**) AR: total L2 ratios highlight differences in allocation of AR cells in gas treatments. (**E**) Transverse reconstructions showing untreated fertile (*center*), O₂ (*left*) and N₂ (*right*) treatment. Central AR cells denoted with pink dots. Scale bar = 15 μm. (**F**) Bilayer progression was delayed in O₂ and slightly accelerated in N₂. In all panels stars represent significance compared to control by Student's T-test ($p < 0.01$). Error bars are +/- s.d. ($N > 10$).

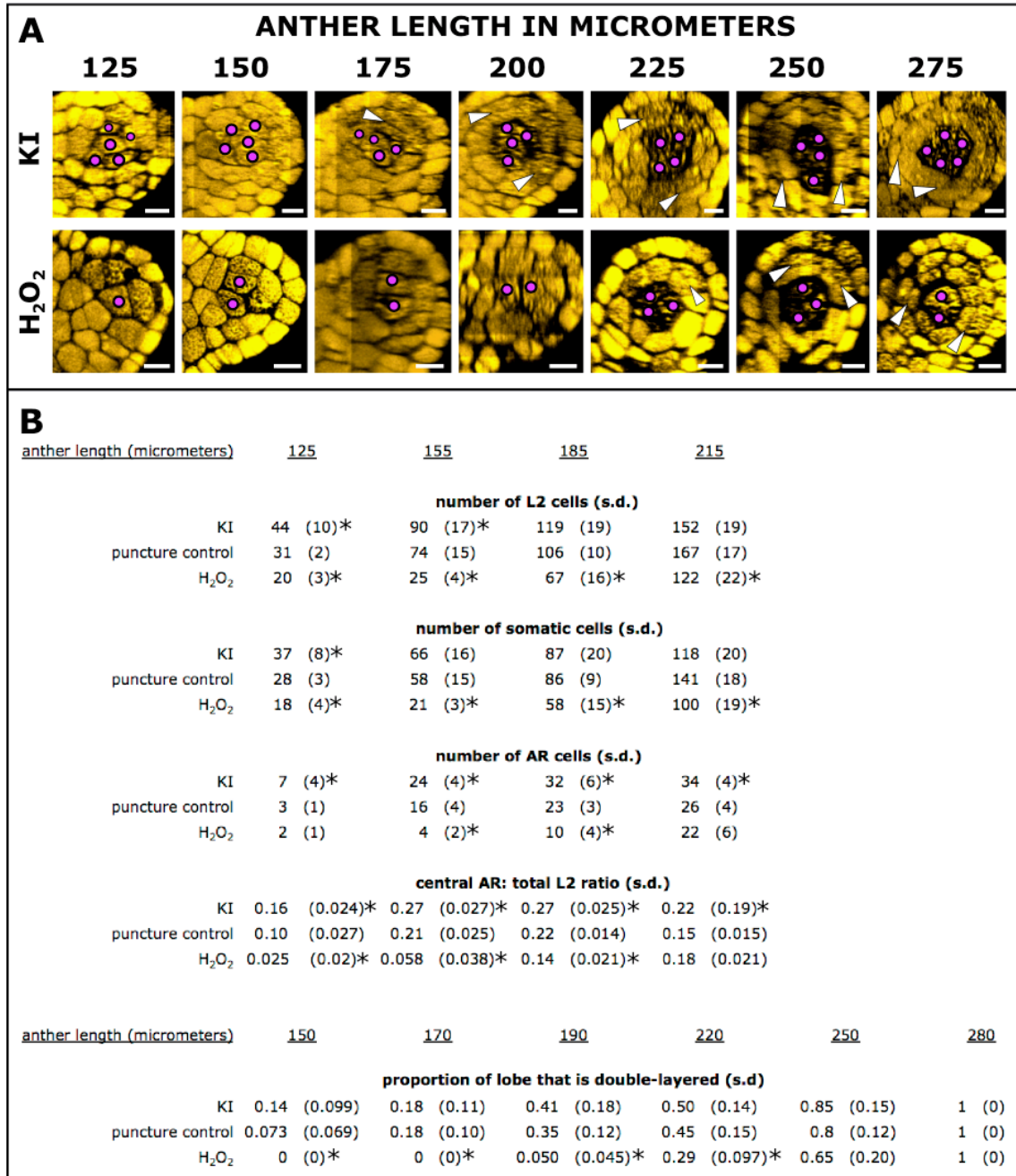


Fig. S12

1 mM H₂O₂ inhibited and 10 mM KI promoted AR cell specification and somatic bilayer development after 48-hour treatments. (A) Transverse reconstructions of KI (top) and H₂O₂ (bottom) treatment with excess AR cells (pink dots) early in KI and precocious bilayer development (white arrowheads). Scale bar = 15 μm. (B) Table showing total L2, somatic, and central AR cell counts, AR: total L2 ratios, and the proportion of the lobe occupied by the somatic bilayer. (top) All treatments promoted cell proliferation of the early lobe compared to untreated, with KI being the most dramatic, H₂O₂ the least. Setting mock injection (wounding via needle puncture) as the control, KI significantly

promoted the formation of AR cells at all four size categories while H₂O₂ significantly inhibited their specification in two of the four. The central AR: total L2 ratio highlights the differences between treatments, with KI preferentially dedicating a higher proportion of cells to the AR population than puncture control and H₂O₂ resulting in a lower proportion in 3 of the 4 size classes. (*bottom*) Bilayer development was slightly accelerated in KI and delayed in H₂O₂. Stars represent significance compared to control by Student's T-test ($p < 0.01$).

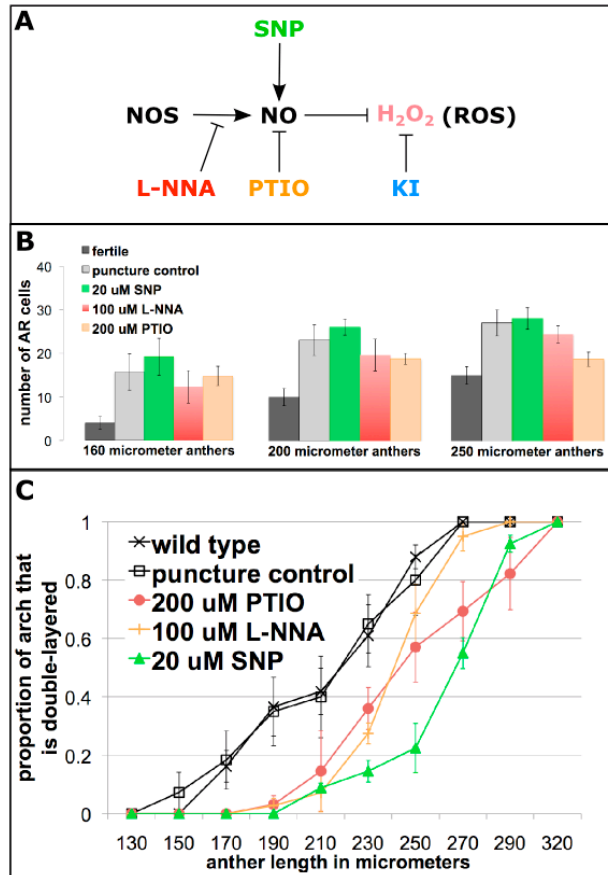


Fig. S13

Nitric oxide (NO) (ROS inhibitor) pushes cells towards an AR fate. (A) N^G-nitro-L-Arginine (L-NNA) (NO synthase inhibitor), 2-Phenyl-4,4,5,5-tetramethylimidazoline-1-oxyl-3-oxide (PTIO) (NO scavenger), and sodium nitroprusside (SNP) (NO donor) were injected into the tassel airspace during the critical AR specification period 48 hours prior to anther dissection. NO suppresses methyl jasmonate-induced H₂O₂ production (17) and reduces O₂ consumption (23). All three treatments slowed the morphological differentiation of central AR cells. Central cells were present but anthers did not achieve the normal somatic ring / central germinal cell organization until ~250 μm. (B) Central AR counts were slightly repressed in PTIO and L-NNA treatments, and slightly promoted in SNP at all three stages checked. (C) The progression of somatic bilayer formation was dramatically delayed in all three treatments compared to the puncture control and untreated plants, with SNP being the most delayed (green). Diphenylene iodonium (DPI) (inhibits NADPH oxidase and other flavin-containing enzymes) was also administered, but this treatment caused complete degeneration of the tassel tissues. Error bars are +/- s.d.

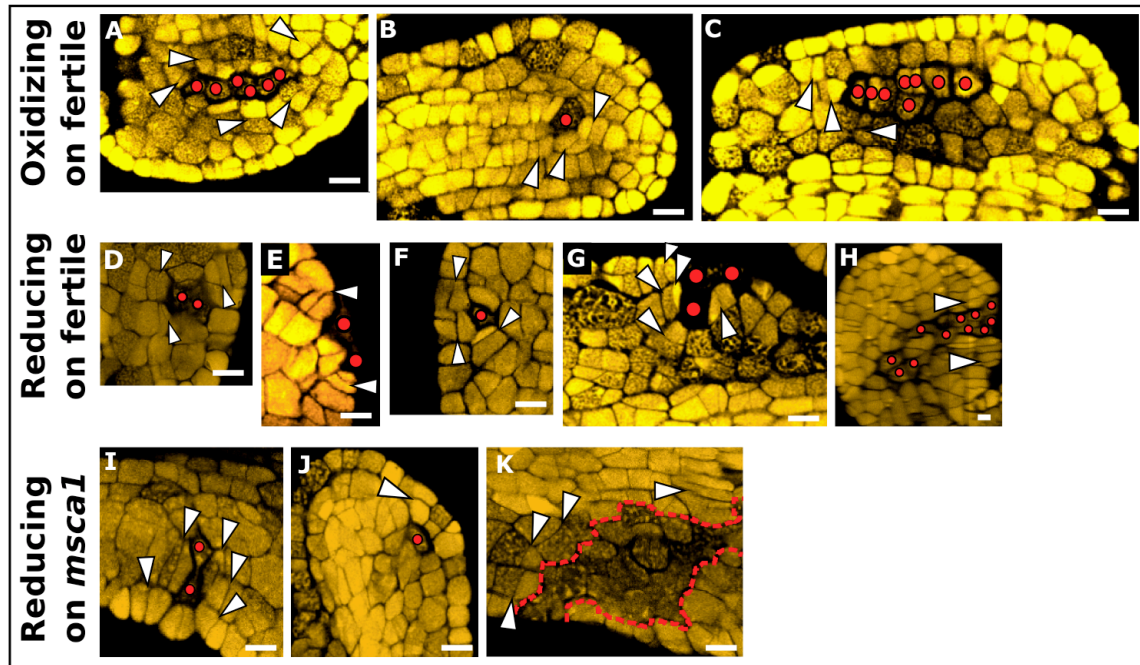


Fig. S14

Additional cases of ectopic archesporial (AR) cells in oxidizing (**A-C**) and reducing (**D-H**) treatments on fertile plants, and in reducing treatments (**I-K**) on *msca1* plants. All ectopic AR (red dots) in these examples stimulated oriented divisions in surrounding cells (white arrowheads). (**A**) Ectopic AR column after O₂ needle treatment in connective tissue. (**B**) Single ectopic AR cell in connective tissue after O₂ needle treatment. (**C**) Ectopic AR column in connective tissue after H₂O₂ treatment. (**D**) Subepidermal ectopic AR accompanied by layer-adding divisions in epidermal and subepidermal neighbors after N₂ needle treatment. (**E**) Duet ectopic AR in epidermis after N₂ needle treatment. (**F**) Subepidermal AR after KI treatment stimulating oriented divisions in epidermal and subepidermal neighbors. (**G**) Three ectopic AR on the epidermis following N₂ needle treatment (**H**) Longitudinal image of ectopic AR cluster extending from epidermis to connective tissues following N₂ needle treatment. (**I**) SNP-treated *msca1* anthers with two ectopic AR. (**J**) KI-treated *msca1* with subepidermal ectopic AR and accompanying periclinal divisions in the epidermis. (**K**) Large cluster of ectopic AR in an SNP-treated *msca1* anther outlined by red dots. Scale bar = 20 μm.

Table S1.

Pre-meiotic (1.0 μ m) archesporial (AR)-enriched transcripts in fertile and *mac1*. Laser microdissected AR cells from mutant and fertile sibling were compared on microarray in duplicate (dye swap). The expression of 297 genes found to be enriched in AR cells (12) (GEO # GS30149) at meiosis (1.5 mm stage) is reported. 96.7% of the time, the expression was found to be roughly equal between *mac1* and the fertile heterozygous sibling. 3.3% of transcripts were present and low in fertile but absent in *mac1*. Gene names correspond to the ID on the Agilent microarray. Data deposited in GEO (#XXXXXX).

(column 1)			(column 2)			(column 3)		
GeneName	+/- AR	-/- AR	GeneName	+/- AR	-/- AR	GeneName	+/- AR	-/- AR
TC306331	1080	265	TC309875	219	108	DR813132	0	0
AI944295	34	51	DN586214	34	62	TC289774	124	190
TC311757	111	184	TC283905	0	0	TC293138	71	68
TC313596	49	163	TC309993	651	519	TC295272	347	335
TC313657	64	70	TC314530	0	0	TC301356	1253	737
TC305266	2383	980	TC281589	80	53	DT943054	84	67
TC308593	55	47	TC298798	1295	612	DT943053	207	81
TC287318	53	53	TC282924	302	183	TC305979	247	148
TC301402	501	220	CF059625	1029	64	TC302216	52	57
TC294630	59	138	TC304331	0	0	TC284771	466	362
TC308047	175	150	TC287674	76	63	TC303615	72	63
CO533393	60	54	TC293448	326	596	TC311135	354	137
TC289712	898	509	TC283790	0	0	TC309440	50	55
BQ163730	798	757	TC312974	71	78	TC289387	215	145
CN844996	0	0	CF019406	156	183	TC281453	727	408
TC279560	100	72	TC280500	126	135	TC286486	124	61
TC296845	273	130	CD447985	101	287	TC288800	314	151
TC289757	0	0	CF626131	31	82	TC297030	0	0
TC281079	397	229	TC313491	415	329	TC303749	0	0
TC284042	215	336	TC292774	11472	8276	TC282058	233	348
TC310354	2602	1752	TC314580	77	0	TC302617	132	63
TC283445	527	425	TC283173	47	44	TC299289	57	47
TC279480	171	265	TC298797	333	153	TC297564	70	84
TC296658	59	48	DR906542	81	94	TC293567	3226	2147
TC309174	74	61	TC283852	140	178	TC280737	41	93
TC284552	83	64	TC305717	0	0	TC280740	43	52
TC302598	95	52	TC309747	304	136	CK787298	0	0
TC282176	394	227	TC301790	158	114	TC308668	58	57
CF633046	77	59	TC285165	273	115	TC298179	92	67
TC308051	40	51	TC311526	2093	2001	DT943270	0	0
TC284526	0	0	TC306072	772	367	TC314427	76	57
TC284637	634	260	TC293449	44	50	TC289341	292	331
TC314658	162	85	TC283691	960	487	TC285412	76	60
TC289172	408	460	TC305158	324	328	TC295182	178	100
TC312972	102	94	DR829208	56	49	TC304232	48	46
TC313076	45	59	TC310683	0	0	TC314544	2161	876
TC284770	52	76	DT647788	60	60	DT946613	159	81
TC306070	95	90	TC306026	127	78	TC307673	447	407
TC303407	0	0	AW231811	46	45	TC312497	0	0

TC295047	646	447	TC289354	138	160	TC293566	2214	1700
TC289727	54	47	TC294269	60	50	TC295697	42	48
TC307255	714	355	TC308574	0	0	TC283769	0	0
TC296050	74	61	CD995221	94	83	TC290945	47	48
TC279580	166	164	TC315488	59	53	TC312299	70	53
TC310105	56	0	TC314126	0	0	TC306976	369	261
TC312091	94	68	TC283431	43	124	DR830496	0	0
CX725290	161	72	TC310688	652	493	TC284316	53	0
TC292021	262	104	TC296255	54	71	TC291853	67	57
TC283684	126	75	TC307982	60	301	TC293263	1005	1568
TC295259	60	48	DR795221	521	345	TC301331	226	187
TC301446	376	218	TC314676	220	185	TC282918	192	128
BG837957	0	0	TC289753	0	0	CO440202	74	57
TC313569	102	57	TC307556	85	69	TC299943	1544	493
TC305399	106	188	TC305157	113	73	TC280985	428	179
DT943243	0	0	TC288590	58	0	TC302095	1306	1327
TC315034	86	68	TC287319	3141	4312	TC284035	57	53
TC287642	202	133	TC284111	760	824	TC297465	792	322
BM340065	0	0	TC291009	372	283	TC310988	113	50
TC314450	40	88	TC307363	287	107	TC309808	59	88
TC295884	0	0	TC295705	176	236	CF040072	192	77
TC301395	1043	471	TC296253	0	0	TC298200	137	72
TC295868	98	140	TC284639	111	203	TC311848	2245	3166
TC295891	0	0	TC290471	2035	1337	TC313084	811	251
TC302888	120	94	TC284496	69	82	DT647408	102	57
TC307873	145	287	TC285351	117	88	TC307549	179	103
TC303479	58	0	TC288463	52	47	CF629011	93	171
TC302844	0	0	TC295239	376	149	TC292387	336	225
TC284163	371	292	TC306328	60	51	TC286746	915	869
TC308672	0	0	CO526721	50	46	TC282507	505	558
TC284146	141	67	DT652253	94	61	CD436448	91	52
TC289458	598	288	TC306547	705	355	TC295587	133	63
TC313835	140	187	TC287826	54	46	TC286055	547	331
TC279806	3854	4642	TC297071	60	70	TC285655	23238	7973
CD995946	0	0	AI692111	388	122	TC314264	184	115
TC310318	98	0	TC302041	57	79	TC293287	188	169
CB280793	1780	353	BG319836	208	229	TC282818	472	250
TC287858	0	0	TC290304	81	53	TC308341	58	0
TC289461	213	55	TC312257	134	56	TC279890	1394	1004
BM378145	388	98	TC287864	183	115	TC304579	560	598
TC279550	2384	600	TC304530	80	94	TC301734	80	46
TC311769	54	48	CD573220	55	0	TC301530	196	85
TC310843	404	440	TC313810	0	0	TC280797	548	179
BM259506	55	92	TC309689	51	52	TC313063	193	160
TC310187	6916	2444	TC291467	187	115	CO441573	408	616
TC296799	81	69	TC286409	176	138	TC297993	160	134
TC300972	53	59	TC298303	1230	404	TC283544	83	64
TC295938	53	46	TC279657	0	0	DN559761	215	146
CF635716	0	0	DT650280	83	110	TC280195	589	526
TC307997	332	209	TC292121	4238	3468	TC284424	1327	444
TC315563	65	59	TC283041	57	0	CA827264	110	0
DT643307	143	162	TC295193	59	0	TC293183	386	213
CB278279	134	82	TC297828	0	0	TC296831	546	314
TC300898	68	50	TC294408	130	64	TC294651	92	77

DT645987	78	79	TC294126	92	64	TC304557	81	56
TC294308	58	63	TC302695	0	0	TC283469	186	120
TC287640	360	583	AM1	77	80	TC310367	116	92
BM500607	0	0	TC283097	696	430	BG841754	143	136
BG319898	0	0	TC292342	238	280	TC306103	0	0
TC315043	136	130	TC311214	86	132	TC307437	96	84

Table S2.

Ectopic archesporial (AR) formation in reducing treatments that increase hypoxia and/or lower H₂O₂. Ectopic AR cells were defined by their morphological similarity to normal AR cells combined with non-locular location. The first two rows give the treatment type and genotype, and the next two rows give the general effects of the treatments on AR counts and bilayer progression. The next two rows give the frequency of observing AR in each treatment / genotype combination. By far the protocol that caused the highest frequency of ectopic AR was the SNP treatment on the *mscal* mutant (37% of anthers had AR). KI on *mscal* (9.5%) and SNP + N₂ on fertile (16.2%) treatments also resulted in a high frequency of ectopic AR. Exogenous N₂ application with the hose protocol did not cause ectopic AR in any anthers; this is a gentler treatment than the direct application of gas through the needle. Next the ectopic AR location was tallied as being either superficial (near or on the epidermis (EPI)) or internal (near or in the connective (CT) and vasculature). In reducing treatments ectopic archesporial cell location was biased for peripheral tissues. Finally, the characteristics of the ectopic archesporial cells are given in the final two rows, including the presence of periclinal divisions generating an endothecium (EN) / secondary parietal layer (SPL) -like bilayer surrounding the AR cells (which were absent in all *mac1* ectopic AR) and the average count of AR cells in each instance.

TREATMENTS		TREATMENTS (REDUCING)												TOTAL
GENOTYPE														
			N₂ (direct)	N₂ (hose)	KI	SNP	N₂ + SNP	N₂ (direct)	KI	SNP	N₂ (direct)	KI	SNP	
			fertile	fertile	fertile	fertile	fertile	<i>mac1</i>	<i>mac1</i>	<i>mac1</i>	<i>msca1</i>	<i>msca1</i>	<i>msca1</i>	
TREATMENT EFFECTS														
	AR count		extra	extra	extra	extra	extra	extra	extra	extra	none	extra	extra	
	SPL/EN timing		early	early	early	delayed	delayed	N/A	N/A	N/A	N/A	N/A	N/A	
COUNT														
	total	anthers	95	88	100	23	37	85	20	15	45	63	30	601
	# having	ectopic AR	4	0	2	1	6	7	0	0	1	6	11	38 (6.3%)
LOCATION														
	by	EPI	4	0	2	1	5	5	0	0	1	5	7	30 (83%)
	by	CT	0	0	0	0	1	2	0	0	0	1	2	6 (17%)
CHARACTERISTICS														
	AR per niche -	forming	Y	N/A	Y	Y	Y	N	N/A	N/A	Y	Y	Y	
	event		5	N/A	7	17	4.2	3	N/A	N/A	1	3	7.5	Avg = 5.4

Table S4.

A subset of premeiotic (600-700 μm) archesporial (AR)-enriched transcripts. Laser-microdissected AR cells were compared in duplicate (dye swap) to whole anthers (WA) from the same tassel at the same stage. Genes that were expressed two-fold higher in AR versus WA have a \log_2 ratio > 0.58 ($p < 0.05$). Some genes just below the cutoff are listed because of their importance to either alternative metabolism or ROS handling. Data deposited in GEO (#XXXXX).

Protein_Match_ID	annotation / description	\log_2 AR/WA	p-value	AR intensity	WA intensity
GRMZM2G020801	aconitate hydratase	2.36	5.50E-07	2344	451.4
GRMZM2G176307	cytosolic glyceraldehyde-3-phosphate dehydrogenase	2.34	3.66E-11	515	104.8
GRMZM5G894515	NAD(P)H-quinone oxidoreductase subunit 5, chloroplast precursor	2.26	3.10E-08	1604	309.8
GRMZM2G060079	oxidoreductase, 2OG-Fe oxygenase family protein	2.10	1.83E-12	235.7	57.5
GRMZM2G368799	inositol hexaphosphate kinase (NADH metabolism)	2.09	7.26E-14	2210.8	517
GRMZM2G415579	NAD(P)H-dependent oxidoreductase	1.75	8.85E-13	419.7	129.5
GRMZM2G473001	Phosphoenolpyruvate carboxylase 2 (PEPCase 2)(PEPC)	1.71	2.42E-12	306.2	91.2
GRMZM2G383088	plastidic 2-oxoglutarate/malate transporter	1.61	1.12E-12	1640.7	586.1
GRMZM5G866223	NAD(P)H-quinone oxidoreductase subunit I, chloroplast precursor	1.51	2.91E-08	13249.2	5437.1
GRMZM5G800096	NAD(P)H-quinone oxidoreductase chain 4, chloroplast precursor	1.39	1.13E-07	2048.7	638.5
GRMZM2G096753	phosphoenolpyruvate carboxylase kinase 3 (PEPCK)	1.37	8.90E-02	1308.5	1048.7
GRMZM2G120857	3-isopropylmalate dehydrogenase	1.14	1.07E-07	646.8	290.2
GRMZM5G800980	NAD(P)H-quinone oxidoreductase subunit K, chloroplast precursor	1.00	1.60E-03	2127.4	1081.6
GRMZM2G113216	thiol oxidoreductase	0.92	1.64E-08	192.4	97.4
GRMZM2G076524	succinate dehydrogenase	0.90	1.35E-09	1807.7	1129
GRMZM2G004847	glutaredoxin subgroup I; Grx_C3	0.82	6.70E-07	129.5	86
GRMZM2G018251	WW domain-containing oxidoreductase (alcohol dehydrogenase)	0.74	8.60E-05	898.1	430.3
GRMZM2G073351	NADPH protochlorophyllide oxidoreductase	0.69	1.34E-06	99.9	65.2
GRMZM2G329144	glutathione peroxidase	0.62	2.20E-04	1149.1	706.8
GRMZM2G051355	alcohol dehydrogenase	0.58	5.08E-06	90.9	58.8
GRMZM2G085019	NADP-dependent malic enzyme, chloroplastic precursor	0.57	1.50E-03	545.1	466.7
GRMZM2G107597	cytochrome c oxidoreductase	0.57	3.50E-05	117.2	70.7

References

1. C. G. Extavour, M. Akam, Mechanisms of germ cell specification across the metazoans: Epigenesis and preformation. *Development* **130**, 5869 (2003). [doi:10.1242/dev.00804](https://doi.org/10.1242/dev.00804) [Medline](#)
2. C. Juliano, G. Wessel, Developmental biology. Versatile germline genes. *Science* **329**, 640 (2010). [doi:10.1126/science.1194037](https://doi.org/10.1126/science.1194037) [Medline](#)
3. C. L. Hord, H. Ma, Genetic control of anther cell division and differentiation. *Plant Cell Monogr* **9**, 361 (2008). [doi:10.1007/7089_2007_136](https://doi.org/10.1007/7089_2007_136)
4. P. A. Bedinger, J. E. Fowler, in *Handbook of Maize: Its Biology*, J. L. Bennetzen, S. C. Hake, Eds. (Springer, New York, 2009), pp. 57–77.
5. R. B. Goldberg, T. P. Beals, P. M. Sanders, Anther development: Basic principles and practical applications. *Plant Cell* **5**, 1217 (1993). [Medline](#)
6. L. C. Boavida, J. D. Becker, J. A. Feijó, The making of gametes in higher plants. *Int. J. Dev. Biol.* **49**, 595 (2005). [doi:10.1387/ijdb.0520191b](https://doi.org/10.1387/ijdb.0520191b) [Medline](#)
7. R. C.-J. Wang *et al.*, *Development* **139**, 2594 (2012).
8. W. F. Sheridan, E. A. Golubeva, L. I. Abrhamova, I. N. Golubovskaya, The *mac1* mutation alters the developmental fate of the hypodermal cells and their cellular progeny in the maize anther. *Genetics* **153**, 933 (1999). [Medline](#)
9. X. Feng, H. G. Dickinson, Tapetal cell fate, lineage and proliferation in the *Arabidopsis* anther. *Dev* **137**, 2409 (2010). [doi:10.1242/dev.049320](https://doi.org/10.1242/dev.049320)
10. C. Albrecht, E. Russinova, V. Hecht, E. Baaijens, S. de Vries, The *Arabidopsis thaliana* SOMATIC EMBRYOGENESIS RECEPTOR-LIKE KINASES1 and 2 control male sporogenesis. *Plant Cell* **17**, 3337 (2005). [doi:10.1105/tpc.105.036814](https://doi.org/10.1105/tpc.105.036814) [Medline](#)
11. X. Feng, H. G. Dickinson, Packaging the male germline in plants. *Trends Genet.* **23**, 503 (2007). [doi:10.1016/j.tig.2007.08.005](https://doi.org/10.1016/j.tig.2007.08.005) [Medline](#)
12. G.-L. Nan *et al.*, Global transcriptome analysis of two ameiotic1 alleles in maize anthers: Defining steps in meiotic entry and progression through prophase I. *BMC Plant Biol.* **11**, 120 (2011). [doi:10.1186/1471-2229-11-120](https://doi.org/10.1186/1471-2229-11-120) [Medline](#)
13. T. Kelliher, V. Walbot, Emergence and patterning of the five cell types of the *Zea mays* anther locule. *Dev. Biol.* **350**, 32 (2011). [doi:10.1016/j.ydbio.2010.11.005](https://doi.org/10.1016/j.ydbio.2010.11.005) [Medline](#)
14. J. L. Leatherman, S. Dinardo, Germline self-renewal requires cyst stem cells and stat regulates niche adhesion in *Drosophila* testes. *Nat. Cell Biol.* **12**, 806 (2010). [doi:10.1038/ncb2086](https://doi.org/10.1038/ncb2086) [Medline](#)
15. M. C. Albertson *et al.*, U.S. patent 7915478 (2011).
16. H. Tsukagoshi, W. Busch, P. N. Benfey, Transcriptional regulation of ROS controls transition from proliferation to differentiation in the root. *Cell* **143**, 606 (2010). [doi:10.1016/j.cell.2010.10.020](https://doi.org/10.1016/j.cell.2010.10.020) [Medline](#)

17. J. W. Wang, J. Y. Wu, Nitric oxide is involved in methyl jasmonate-induced defense responses and secondary metabolism activities of *Taxus* cells. *Plant Cell Physiol.* **46**, 923 (2005). [doi:10.1093/pcp/pci098](https://doi.org/10.1093/pcp/pci098) [Medline](#)
18. G. Bertoni, CBS domain proteins regulate redox homeostasis. *Plant Cell* **23**, 3562 (2011). [doi:10.1105/tpc.111.231011](https://doi.org/10.1105/tpc.111.231011) [Medline](#)
19. S. Li *et al.*, Nuclear activity of ROXY1, a glutaredoxin interacting with TGA factors, is required for petal development in *Arabidopsis thaliana*. *Plant Cell* **21**, 429 (2009). [doi:10.1105/tpc.108.064477](https://doi.org/10.1105/tpc.108.064477) [Medline](#)
20. J. Murmu *et al.*, Arabidopsis basic leucine-zipper transcription factors TGA9 and TGA10 interact with floral glutaredoxins ROXY1 and ROXY2 and are redundantly required for anther development. *Plant Physiol.* **154**, 1492 (2010). [doi:10.1104/pp.110.159111](https://doi.org/10.1104/pp.110.159111) [Medline](#)
21. L. Hong *et al.*, Somatic and reproductive cell development in rice anther is regulated by a putative glutaredoxin. *Plant Cell* **24**, 577 (2012). [doi:10.1105/tpc.111.093740](https://doi.org/10.1105/tpc.111.093740) [Medline](#)
22. Q. Chen, E. J. Vazquez, S. Moghaddas, C. L. Hoppel, E. J. Lesnefsky, Production of reactive oxygen species by mitochondria: Central role of complex III. *J. Biol. Chem.* **278**, 36027 (2003). [doi:10.1074/jbc.M304854200](https://doi.org/10.1074/jbc.M304854200) [Medline](#)
23. G. Miller, V. Shulaev, R. Mittler, Reactive oxygen signaling and abiotic stress. *Physiol. Plant.* **133**, 481 (2008). [doi:10.1111/j.1399-3054.2008.01090.x](https://doi.org/10.1111/j.1399-3054.2008.01090.x) [Medline](#)
24. J. Bagañá, E. Saló, C. Auladell, *Development* **107**, 77 (1989).
25. M. V. Gustafsson *et al.*, Hypoxia requires notch signaling to maintain the undifferentiated cell state. *Dev. Cell* **9**, 617 (2005). [doi:10.1016/j.devcel.2005.09.010](https://doi.org/10.1016/j.devcel.2005.09.010) [Medline](#)
26. B. Keith, M. C. Simon, Hypoxia-inducible factors, stem cells, and cancer. *Cell* **129**, 465 (2007). [doi:10.1016/j.cell.2007.04.019](https://doi.org/10.1016/j.cell.2007.04.019) [Medline](#)
27. S. J. Morrison *et al.*, Culture in reduced levels of oxygen promotes clonogenic sympathoadrenal differentiation by isolated neural crest stem cells. *J. Neurosci.* **20**, 7370 (2000). [Medline](#)
28. J. Ma, D. S. Skibbe, J. F. Fernandes, V. Walbot, *Genome Biol.* **9**, R181 (2008).
29. W. C. Yang, D. Ye, J. Xu, V. Sundaresan, The *SPOROCTELESS* gene of *Arabidopsis* is required for initiation of sporogenesis and encodes a novel nuclear protein. *Genes Dev.* **13**, 2108 (1999). [doi:10.1101/gad.13.16.2108](https://doi.org/10.1101/gad.13.16.2108) [Medline](#)
30. C. Canales, A. M. Bhatt, R. Scott, H. Dickinson, EXS, a putative LRR receptor kinase, regulates male germline cell number and tapetal identity and promotes seed development in *Arabidopsis*. *Curr. Biol.* **12**, 1718 (2002). [doi:10.1016/S0960-9822\(02\)01151-X](https://doi.org/10.1016/S0960-9822(02)01151-X) [Medline](#)
31. G. Jia, X. Liu, H. A. Owen, D. Zhao, Signaling of cell fate determination by the TPD1 small protein and EMS1 receptor kinase. *Proc. Natl. Acad. Sci. U.S.A.* **105**, 2220 (2008). [doi:10.1073/pnas.0708795105](https://doi.org/10.1073/pnas.0708795105) [Medline](#)

32. K. Nonomura *et al.*, The *MSP1* gene is necessary to restrict the number of cells entering into male and female sporogenesis and to initiate anther wall formation in rice. *Plant Cell* **15**, 1728 (2003). [doi:10.1105/tpc.012401](https://doi.org/10.1105/tpc.012401) [Medline](#)
33. D. Z. Zhao, G. F. Wang, B. Speal, H. Ma, The *EXCESS MICROSPOROCTES1* gene encodes a putative leucine-rich repeat receptor protein kinase that controls somatic and reproductive cell fates in the *Arabidopsis* anther. *Genes Dev.* **16**, 2021 (2002). [doi:10.1101/gad.997902](https://doi.org/10.1101/gad.997902) [Medline](#)